ORIGINAL ARTICLE

Introduction of TROPS ionospheric TEC products for FORMOSAT-7/COSMIC-2 mission

Wen-Hao Yeh[1*], Cheng-Yung Huang[1], Kun-Lin Chen[1], Tzu-Pang Tseng[2], Tung-Yuan Hsiao[3], Hsu-Hui Ho[4], Jing-Mei Wu[5], Jyun-Ying Huang[4], Hsiu-Wen Li[5], Ching-Chieh Lin[4], I.-Te Lee[6] and Tie-Yue Liu[1]

Abstract

Six low Earth orbit (LEO) satellites were launched on June 25th, 2019 for a radio occultation (RO) mission for the FORMOSAT-7/COSMIC-2 (F7/C2) program. The GPS and GLONASS RO signals received by these F7/C2 satellites can be used to retrieve atmospheric and ionospheric parameter profiles for atmospheric and ionospheric research. In order to process the received RO signal, the processing system named Taiwan Radio Occultation Processing System (TROPS) is built. TROPS is developed by National Space Organization, Taiwan Analysis Center for COSMIC, and GPS Science and Application Research Center in Taiwan. The ionospheric products of TROPS are electron density profile, ionospheric scintillation index (S4 index), and absolute total electron content (TEC). S4 index has been calculated on board the satellites and other two products are retrieved by TROPS after the observation data downlink to ground. TEC is the linear integration of electron density along the signal propagation path. The electron density profile is retrieved from the relative TEC when the elevation angle of GNSS satellite is negative from F7/C2 satellite. The absolute TEC is the TEC from GNSS satellite to F7/C2 satellite. The difference between absolute and relative TEC is the TEC with/without differential code bias (DCB) correction. Currently, the data for the electron density profile and absolute TEC are provided by TROPS. Users can obtain the products freely from the internet. In this study, the retrieval method and the preliminary F7/C2 ionospheric TEC products retrieved by TROPS are presented in detail.

Key points

(1) Electron density profiles data service of FORMOSAT-7/COSMIC-2.
(2) Absolute TEC data service of FORMOSAT-7/COSMIC-2.
(3) Validation results confirms the data is ready to use.

Keywords: Radio occultation (RO), FORMOSAT-7/COSMIC-2, Taiwan Radio Occultation Process System (TROPS), Total electron content (TEC)

1 Introduction

The Taiwan Radio Occultation Processing System (TROPS) was developed for data processing and retrieval for the FORMOsa SATellite Mission-7/Constellation Observing System for Meteorology, Ionosphere, and Climate-2 (FORMOSAT-7/COSMIC-2, F7/C2) program, which is an international collaboration between the National Space Organization (NSPO) of Taiwan and the National Oceanic and Atmospheric Administration

*Correspondence: s681231@gmail.com

[1] National Space Organization, National Applied Research Laboratories, Hsinchu, Taiwan
Full list of author information is available at the end of the article

Yeh *et al. Terrestrial, Atmospheric and Oceanic Sciences* (2022) 33:23

Page 2 of 9

(NOAA) of the United States, launched on June 25th, 2019. F7/C2 is a follow up to the FORMOsa SATellite Mission-3/Constellation Observing System for the Meteorology, Ionosphere, and Climate (FORMOSAT-3/COSMIC, F3/C) program (Fong et al. 2008), which is also an international collaborative effort between NSPO and the University Corporation for Atmospheric Research (UCAR) of the United States. F3/C was the first weather satellite mission in Taiwan with six low Earth orbit (LEO) satellites and was launched in 2006. The F3/C products allowed the generation of atmospheric and ionospheric parameter profiles by using radio occultation (RO) technique (Schreiner et al. 1999; Wickert et al. 2001).

The mission payload of F3/C, the GPS Occultation Experiment (GOX), was used for RO observation and to receive Global Positioning System (GPS) signals for retrieval of the atmospheric and ionospheric parameter profiles and can provide around 2000 pressure, temperature, and electron density profiles per day. Due to the success of F3/C, the F7/C2 program was later developed. The mission payload of F7/C2, Tri-GNSS Radio Occultation System (TGRS) can not only receive GPS signals but also GLObal NAvigation Satellite System (GLONASS) for RO observation. The F7/C2 data products are similar to F3/C's but the generated data volume is about twice that of F3/C. The ionospheric products of the F3/C GOX payload have been used for the study of ionospheric activity (Lin et al. 2010; Liu et al. 2010; Chang et al. 2014), space weather nowcasting (Lin et al. 2015, 2017) and forecasting (Lee et al. 2012; Hsu et al. 2014), as well as detection of ionospheric irregularities (Yeh et al. 2012, 2014; Liu et al. 2016; Chen et al. 2017), and plasmaspheric activity (Chen 2008; Cherniak et al. 2012). Due to the difference in the orbital inclination angle, from 72° for the F3/C satellites to 24° for the F7/C2 satellite, the data distribution of the F7/C2 TGRS is roughly between 45° N to 45° S. Although the data distribution of F7/C2 only includes the mid- and lower-latitudes, the density is around 4 times that of F3/C, because of having double the data volume and half the distribution area. The ionospheric products of F7/C2 allow more detailed ionospheric research studies.

In order to thoroughly understand the process of the data retrieval and achieve the data latency required by the F7/C2 mission, it is necessary to obtain as much information as possible for data applications. TROPS was developed as a joint effort between NSPO, Taiwan Analysis Center for COSMIC (TACC) of Central Weather Bureau (CWB), and GPS Science and Application Research Center (GPSARC) at National Central University (NCU) in Taiwan. The architecture of TROPS is shown in Fig. 1. The architecture is divided into three main segments for data collection, data processing, and

data service, shown on the left, top right, and bottom right sides of Fig. 1, respectively. In data processing portion, the blue ovals indicate the modules for precision orbit determination (POD) and green ones are for atmospheric and ionospheric data retrieving. The POD modules are not only for Global Navigation Satellite System (GNSS) and LEO satellites' POD but also for the calculation of intermediate data, such as the satellite clock offset (Tseng et al. 2018). The main products of the atmospheric data retrieving module are the pressure, temperature, and water vapor profiles. The main products of the ionospheric data retrieving module are the electron density profile, ionospheric scintillation S4 index (S4 index), and absolute total electron content (TEC). Since the S4 index is calculated on board the satellite and does not need to be retrieved, the S4 index of TROPS has been compared with the results of COSMIC Data Analysis and Archive Center (CDAAC) retrieval system operated in TACC to confirm the offset and scaling factors for file transferring by using ~O(10) observations. Only the details of electron density profile, which is retrieved from relative TEC, and absolute TEC retrieval process module are presented in this study. The difference between relative and absolute TEC is the TEC without/with difference code bias (DCB) correction.

The retrieval method used in the module is described in Sect. 2. The retrieval results are displayed, followed by the conclusions.

2 Highlights of FORMOSAT-3/COSMIC retrieval methods

The ionospheric RO observations are illustrated in Fig. 2. The signal is transmitted from the left side GNSS satellites (G_1–G_4) and propagates through Earth's ionosphere, then it is received by the TGRS of F7/C2 satellite (point F_1–F_4). The influence of the received GNSS signal by the ionosphere is presented in the phase and amplitude of the received signal. The dual band of the GNSS signal and the different frequency causes a difference in the refractive index when the signal propagates through a medium with the same electron density. The total electron content (TEC) can be calculated from observed pseudorange (TEC_p) and carrier phase (TEC_c) by

$$TEC_p = \frac{1}{40.31} \left(\frac{f_1^2 f_2^2}{f_1^2 - f_2^2} \right) (P_2 - P_1 - k_t - k_r) \quad \text{(1a)}$$

$$TEC_c = \frac{1}{40.31} \left(\frac{f_1^2 f_2^2}{f_1^2 - f_2^2} \right) [\lambda_1 (S_1 + N_1) - \lambda_2 (S_2 + N_2)] \quad \text{(1b)}$$

where λ_1, λ_2, N_1, N_2, k_t, k_r, f_1, f_2, P_1, P_2, S_1, and S_2, are wavelength of L1 band, wavelength of L2 band,
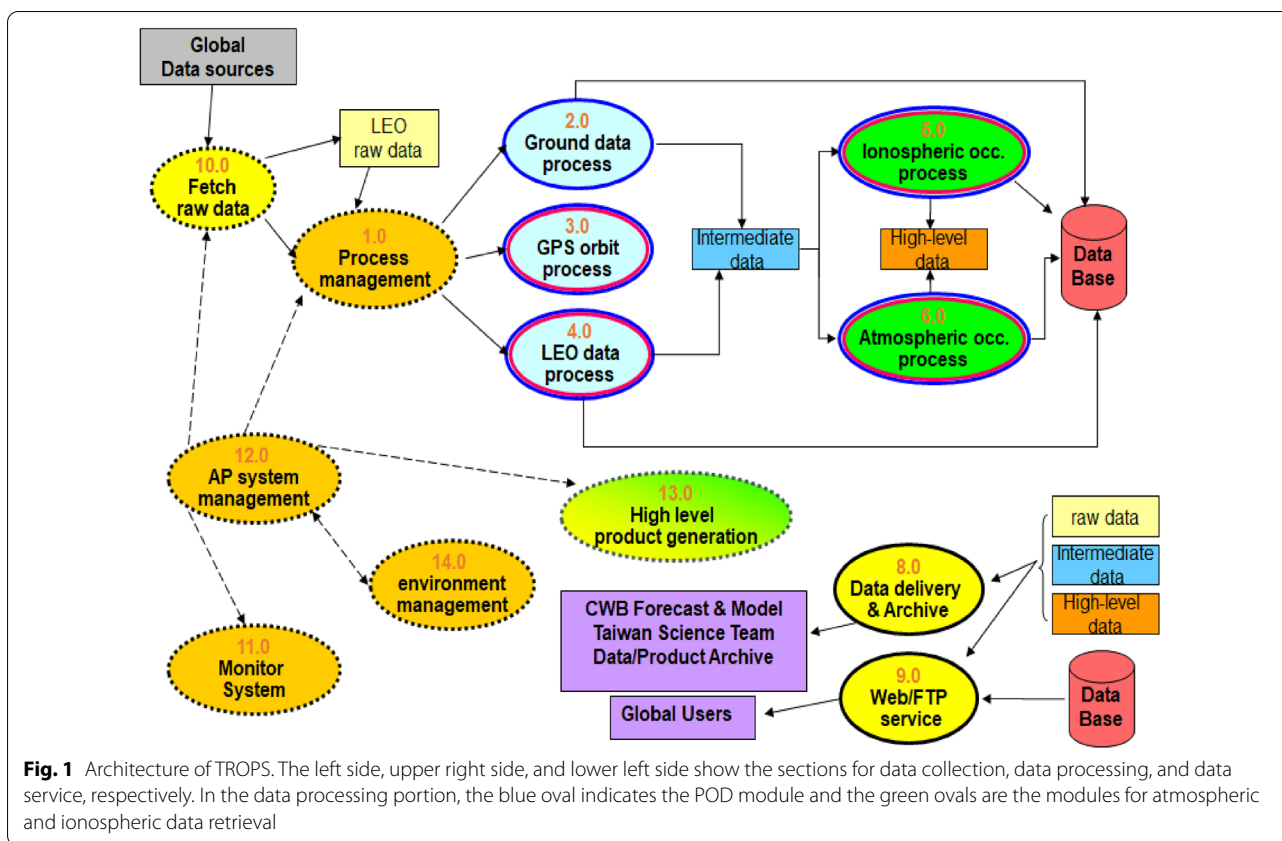
Fig. 1 Architecture of TROPS. The left side, upper right side, and lower left side show the sections for data collection, data processing, and data service, respectively. In the data processing portion, the blue oval indicates the POD module and the green ovals are the modules for atmospheric and ionospheric data retrieval
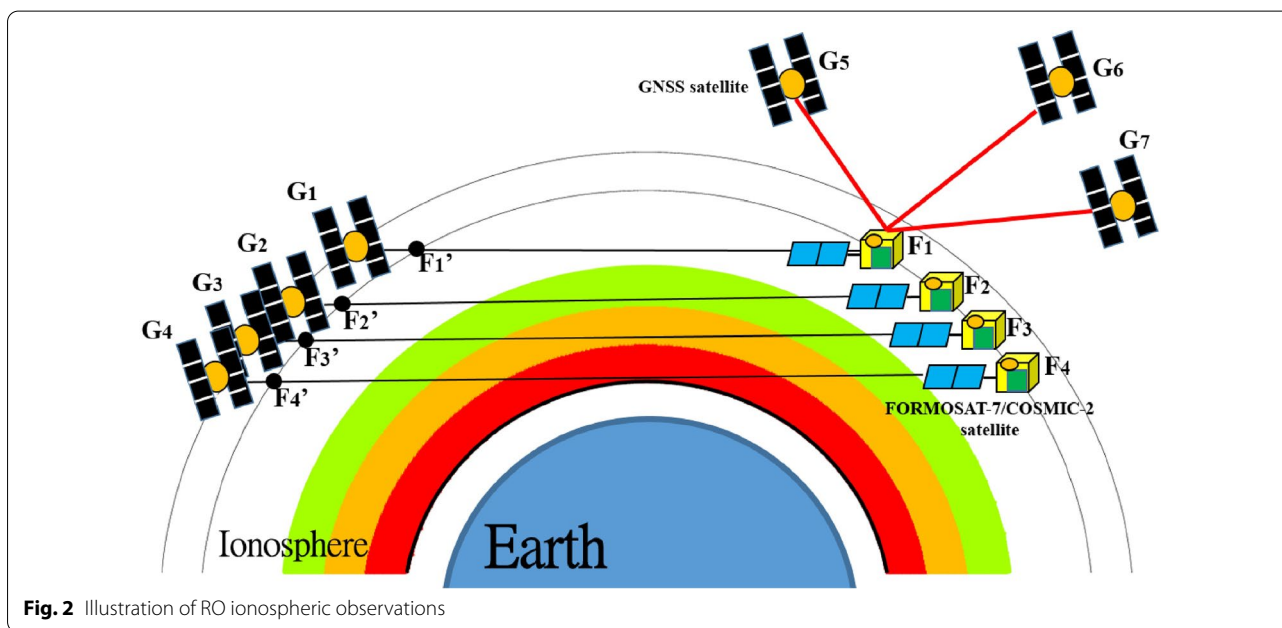

Fig. 2 Illustration of RO ionospheric observations

ambiguity of L1 band, ambiguity of L2 band, differential code bias (DCB) of transmitter, DCB of receiver, the frequency of the L1 band, the frequency of the L2 band, the pseudorange of L1 band, the pseudorange of L2 band, the carrier L1 phase, and the carrier L2 phase, respectively (Liu et al. 1996). The TEC from

Yeh *et al. Terrestrial, Atmospheric and Oceanic Sciences* (2022) 33:23

Page 4 of 9

point G_1 to point F_1 (TEC_{G1F1}) and point G_1 to point F_1' ($TEC_{G1F1'}$) can be calculated by Eq. (1). The TEC from point F_1' to point F_1 ($TEC_{F1'F1}$) can be calculated by ($TEC_{F1'F1}$) = (TEC_{G1F1}) − ($TEC_{G1F1'}$). Note that TEC_{G1F1} and $TEC_{G1F1'}$ are relative to TEC, which does not remove the influence of the signal ambiguity and DCB. Since the ambiguity and DCB in one arc observation (from point F_1' to point F_1) is the same, (TEC_{G1F1}) − ($TEC_{G1F1'}$) can remove the influence of the signal ambiguity and DCB. In Fig. 2, points F_1' to F_4' are the reference points for F_1 to F_4, respectively. Furthermore, F_1 to F_4 are in the same LEO satellite orbit and $TEC_{F1'F1}$, $TEC_{F2'F2}$, $TEC_{F3'F3}$, and $TEC_{F4'F4}$ can be derived from one arc observation. Although only 4 TECs between the position of the LEO satellite and its reference point are derived with the signal propagating through different altitudes in Fig. 2, several hundred TECs can be derived from real RO observations. Under the assumption that the ionosphere is spherically symmetrical, the Abel transform (Phinney and Anderson 1968), which is often used to analyze spherically symmetric functions, is applied to transfer the TEC profile to the electron density profile. The Abel transform equation for

remains constant during the period of observation and indicated by N_1 and N_2 in Eq. (1b), and the DCB, which is the systematic bias between two GNSS code observations and indicated by k_t and k_r in Eq. (1a), before calculating the TEC. The DCB is calculated from the POD side of the GNSS signal from the last 3 days. Due to the signal of GPS being based on code division multiple access (CDMA) and GLONASS being based on frequency division multiple access (FDMA), the DCB calculation of GPS and GLONASS are different. For GPS signal, the transmitter DCB, which is k_t in Eq. (1a), from the Center for Orbit Determination in Europe (CODE) is used. The receiver DCB of GPS signal, which is k_r in Eq. (1a), is calculated from the several GPS satellite signals received by F7/C2 at the same time. The pseudorange of GPS L2 has two signal types, some satellites are L2P and others are L2C. If the pair of GPS signals is of the same signal type, this pair is chosen for the DCB calculation. Several dozen to several hundred pairs are chosen for DCB calculation for each signal type for each F7/C2 satellite. The DCB is calculated by using the following equation (Yue et al. 2011):

$$DCB = \frac{-\sum_i \left[(mapf(\theta_1) - mapf(\theta_2)) \times (TEC_1 \times mapf(\theta_1) - TEC_2 \times mapf(\theta_2)) \right]}{\sum_i \left(mapf(\theta_1) - mapf(\theta_2) \right)^2} \tag{3}$$

electron density derived from the TEC is (Schreiner et al. 1999)

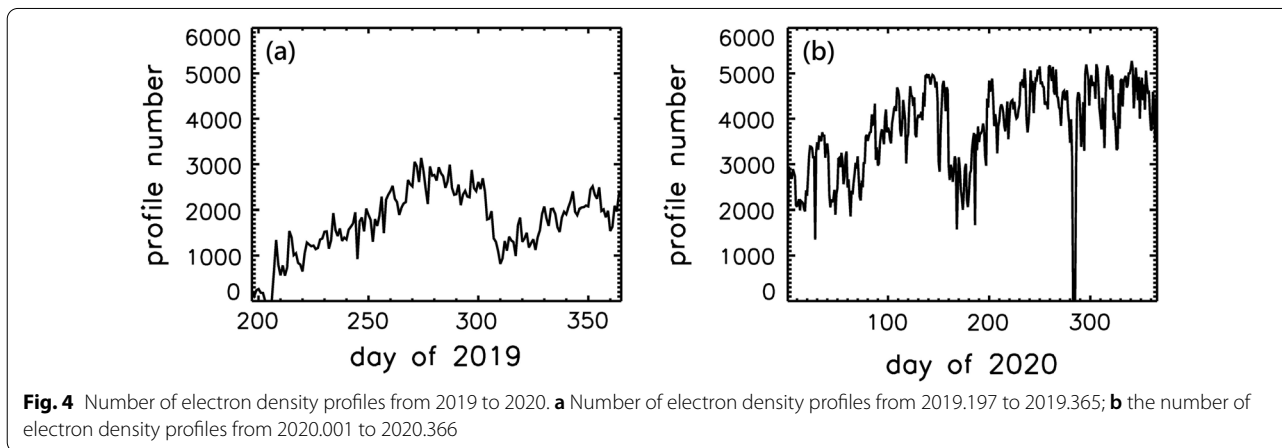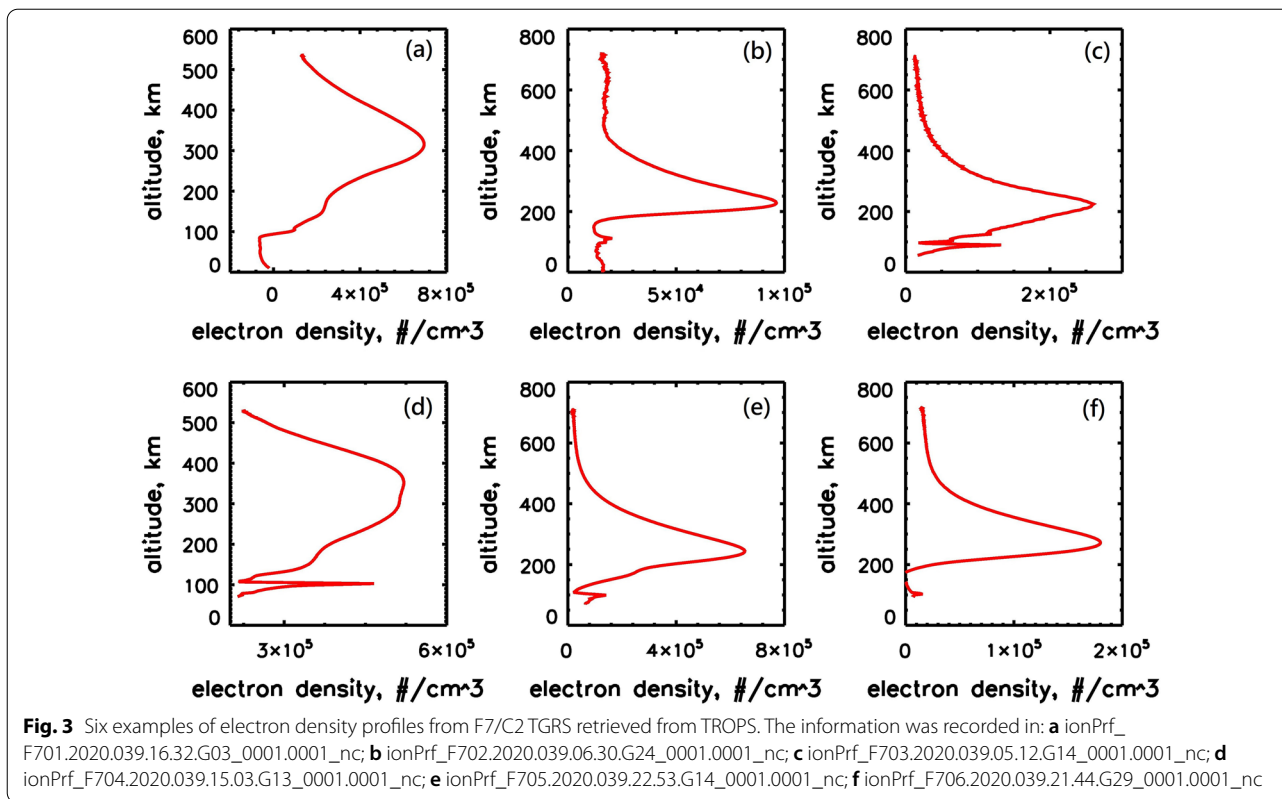$$N(r) = -\frac{1}{\pi} \int_r^{r_{LEO}} \frac{dT/dp}{\sqrt{p^2 - r^2}} dp \tag{2}$$

where N, T, p, r, and r_{LEO} are the electron density, TEC (the TEC between the LEO position and its reference point), altitude, the altitude of the retrieval electron density, and the altitude of the LEO satellite, respectively.

The GNSS satellites (G1 to G4) on the left side in Fig. 2 are on the RO side. The elevation angle of the GNSS satellites from F7/C2 is negative, and their signals can be used to retrieve the electron density profiles. The F7/C2 TGRS not only receives the GNSS signals from the RO side but also from POD side, where the elevation angle of the GNSS satellites from F7/C2 is positive; Satellites G5 to G7 are shown on the right hand side in Fig. 2. The signal received on the POD side of the GNSS satellites is used for POD and also can be used for the calculation of the TEC along the signal propagation path. The TEC can be calculated by using Eq. (1). However, it is necessary to remove the influence of ambiguity, which is the integer refers to the first epoch of observations and

where θ and *mapf* are the elevation angle of the GPS satellite from F7/C2 and the mapping function, respectively. The mapping function is from Foelsche and Kirchengast (2002)

$$mapf(\theta) = \frac{sin\theta + \sqrt{\left(\frac{r_{ion}}{r_{orb}}\right)^2 - (cos\theta)^2}}{1 + \frac{r_{ion}}{r_{orb}}} \tag{4}$$
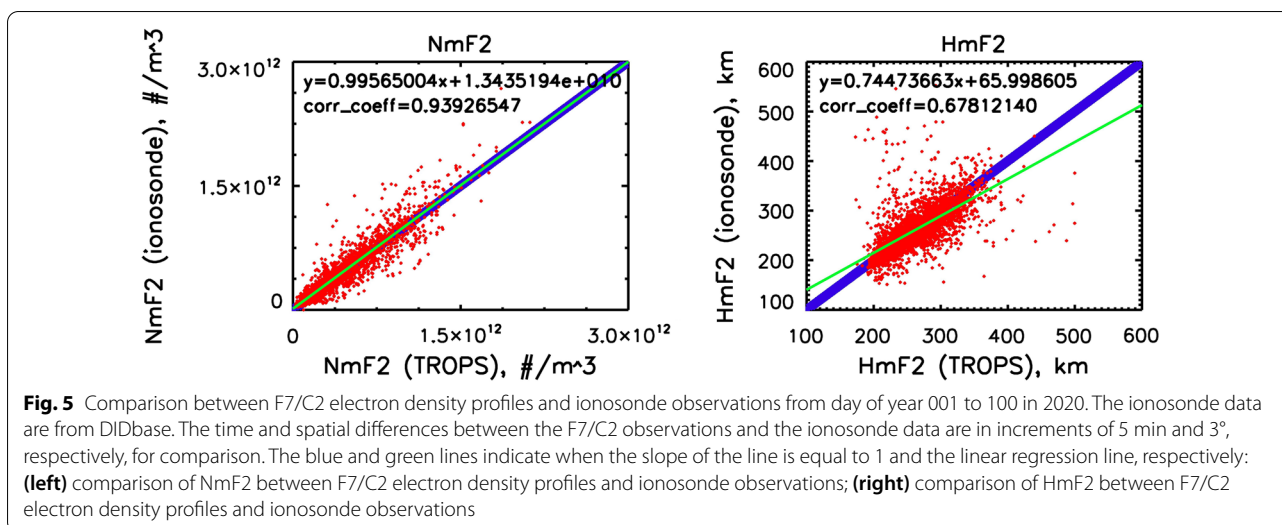
where r_{ion} and r_{orb} are the ionospheric and satellite altitude from the Earth's center. r_{ion} can be selected to be several hundreds or thousands of kilometres above r_{orb} (Yue et al. 2011) and $r_{orb} + 200$ km is used in TROPS. For GLONASS signal, Eqs. (3) and (4) are also used for calculation of DCB, but TEC_1 and TEC_2 are calculated from the same GLONASS satellite at different times with *mapf(θ₁)* and *mapf(θ₂)* as the corresponding mapping function. The calculation results of GLONASS DCB is the summation of k_t and k_r. On the other hand, the ambiguity of L1 and L2 band in Eq. (1b) is the least square results of $N_i = (P_i - \lambda_i S_i - 2d_{ion})/\lambda_i$, i = 1, 2 implies L1 and L2 band, in one arc observation and $d_{ion} = 40.3 TEC_c/f_i^2$ is ionospheric delay. After calculating ambiguity and DCB, the absolute TEC can be derived by Eq. (1).

Fig. 3 Six examples of electron density profiles from F7/C2 TGRS retrieved from TROPS. The information was recorded in: **a** ionPrf_F701.2020.039.16.32.G03_0001.0001_nc; **b** ionPrf_F702.2020.039.06.30.G24_0001.0001_nc; **c** ionPrf_F703.2020.039.05.12.G14_0001.0001_nc; **d** ionPrf_F704.2020.039.15.03.G13_0001.0001_nc; **e** ionPrf_F705.2020.039.22.53.G14_0001.0001_nc; **f** ionPrf_F706.2020.039.21.44.G29_0001.0001_nc

Fig. 4 Number of electron density profiles from 2019 to 2020. **a** Number of electron density profiles from 2019.197 to 2019.365; **b** the number of electron density profiles from 2020.001 to 2020.366

3 FORMOSAT-7/COSMIC-2 mission status retrieval results and discussion
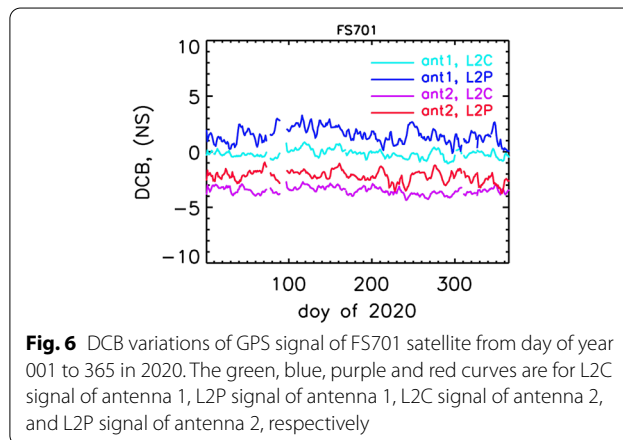
Six examples of electron density profiles in the day of year 2020.039 are shown in Fig. 3. The altitude range of the retrieval electron density profile is from several tens of kilometers to the satellite altitude. The profiles in panel (a) to (f) are from satellites FS701 to FS706. At day of year 2020.039, FS701 and FS704 are at the mission altitude and the others are at the original altitudes, which are 550 km and 720 km, respectively. So, the highest altitude

of the profiles in panels (a) and (d) is around 550 km and the others are around 720 km. The profiles in Fig. 3 show the obvious F region which F2-layer peak density (NmF2) and height (HmF2) are 10^5 to 7×10^5/cm^3 in density and around 200 to 400 km in altitude. In panels (b), (c), (d), and (e) of Fig. 3, the sporadic E (Es) layer occur in the profiles around 100 km in altitude. The electron density of Es layer in panels (c) and (d) is up to around half and full NmF2, respectively. However, due to the assumption of Abel transform, the spherically symmetric electron

Yeh *et al. Terrestrial, Atmospheric and Oceanic Sciences*   (2022) 33:23

Page 6 of 9

Fig. 5 Comparison between F7/C2 electron density profiles and ionosonde observations from day of year 001 to 100 in 2020. The ionosonde data are from DIDbase. The time and spatial differences between the F7/C2 observations and the ionosonde data are in increments of 5 min and 3°, respectively, for comparison. The blue and green lines indicate when the slope of the line is equal to 1 and the linear regression line, respectively: **(left)** comparison of NmF2 between F7/C2 electron density profiles and ionosonde observations; **(right)** comparison of HmF2 between F7/C2 electron density profiles and ionosonde observations

density in ionosphere, the negative value occurs in profiles in profiles in low altitude, like the profile in panel (a).

The variation in the daily amount of electron density profile in 2019 and 2020 is shown in Fig. 4. As can be seen in Fig. 4, F7/C2 can provide around four thousand and sometimes up to five thousand electron density profiles per day if all six satellites are working. A comparison between the F7/C2 electron density profiles and ionosonde observations from day of year 001 to 100 in 2020 is shown in Fig. 5. The NmF2 and HmF2 are used for the comparisons. The ionosonde observations are from the Digital Ionogram Data Base (DIDBase). The time and spatial difference between the F7/C2 and ionosonde observations are 5 min and 3°, respectively, and a total of around 3250 pairs of F7/C2 and ionosonde observations are compared. The blue and green lines in Fig. 5 indicate the lines where the slope is equal to 1 and the linear regression line, respectively. The green line in Fig. 5a is very close to the blue line and the NmF2 of F7/C2 and ionosonde is in good agreement. The green line in Fig. 5b is not as close as to the blue line in Fig. 5a and HmF2 of F7/C2 and ionosonde is not in good agreement as NmF2. The disagreement of HmF2 between F7/C2 and ionosonde is due to ionosonde cannot directly scale the true HmF2 from ionograms and only provide the measurement of the virtual height. The HmF2 provided by ionosonde is derived by the variation of electron density with height is parabolic with plasma frequency under the assumption of a simple ionospheric layer, or by the conversion of a plasma frequency versus virtual height curve to an electron density true height profile (Tsai et al. 2009). Although the agreement of HmF2 is not as good as NmF2 between F7/C2 and ionosonde, the positive slope of regression line and the linear distribution of the red

Fig. 6 DCB variations of GPS signal of FS701 satellite from day of year 001 to 365 in 2020. The green, blue, purple and red curves are for L2C signal of antenna 1, L2P signal of antenna 1, L2C signal of antenna 2, and L2P signal of antenna 2, respectively

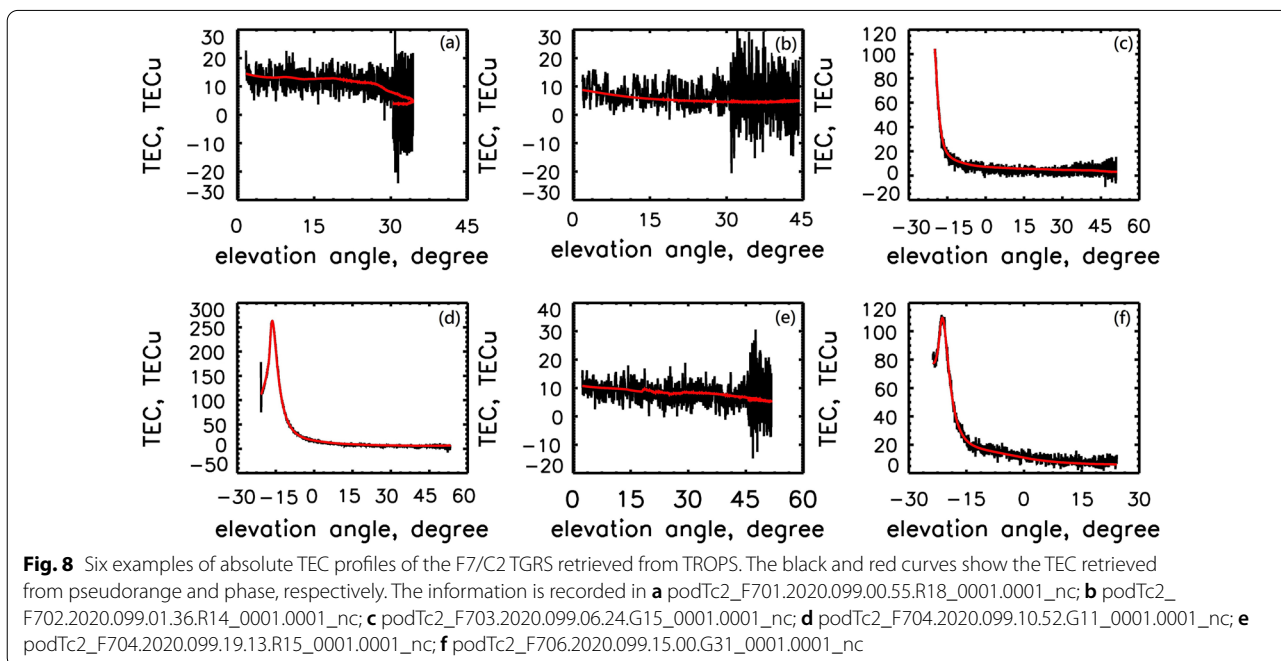dots can validate the TROPS retrieval electron density profile.

Two examples of the GNSS signal DCB are shown in Figs. 6 and 7. The green, blue, purple, and red curves in Fig. 6 show the variations of DCB for the L2C signal of antenna 1, L2P signal of antenna 1, L2C signal of antenna 2, and L2P signal of antenna 2, respectively, of the F7/C2 FS701 satellite, from day of year 001 to 365 in 2020. As can be seen in Fig. 6, the variation of the GPS L2C and L2P signal DCB of F7/C2 FS701 antennas 1 and 2 is stable, with a maximum of around 2 NS perturbations and the trends are around − 1 NS in 1 year. The colored curves in Fig. 7a and b indicate the DCB variations of GLONASS R01 to R26 satellite signals of antenna 1 and 2, respectively, for the F7/C2 FS706 satellite, from day of year 001 to 080 in 2020. As can be seen in Fig. 7, the variation of the GLONASS signal DCB, like of the GPS, is stable with perturbations. The colored curves in Fig. 7b

Fig. 7 DCB variations of GLONASS signal of F7/C2 FS706 satellite from day of year 001 to 080 in 2020. Panel (**a**) and (**b**) are for antenna 1 and antenna 2, respectively
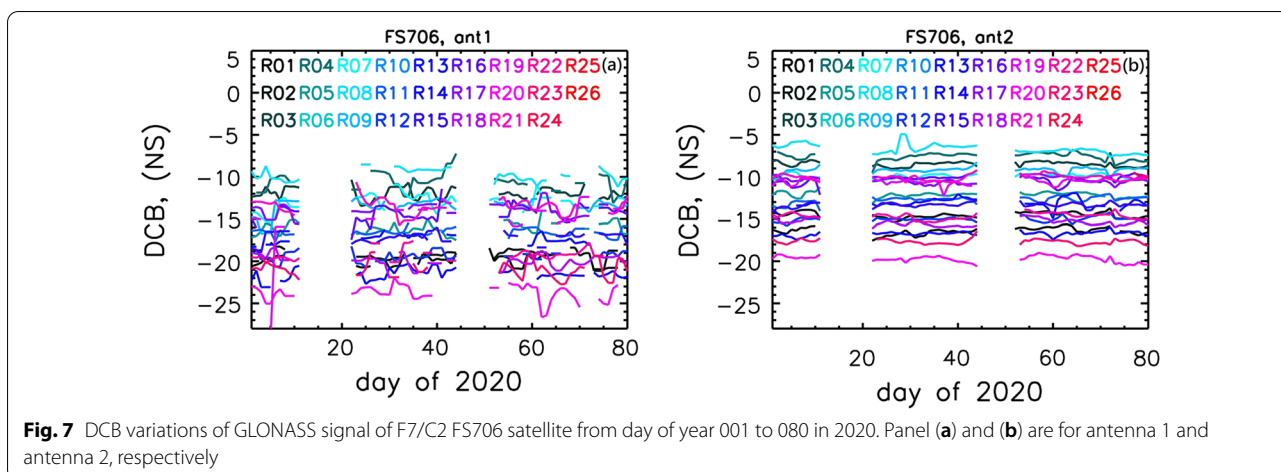
show the maximum variation of the DCB of the GLO-NASS satellite signal for antenna 2 is around 2 NS. However, as shown in Fig. 7a, the perturbation of the variation in the DCB of the GLONASS satellite signal is larger for antenna 1 than antenna 2, up to a maximum of around 4 NS. The higher perturbation shown by the colored curves in Fig. 7a than in Fig. 7b is due to fewer observations for analysis for F7/C2 FS706 antenna 1 than antenna 2. In early 2020, before the TGRS software was updated, the ability of TGRS to receive GLONASS signals was not as good as it is today, so most of the observations for antenna 1 were for rising RO, which is more difficult to receive GLONASS signal than setting RO for antenna 2.

The gaps in Figs. 6 and 7 are due to no observations for analysis when the TGRS power was off.

Six examples of retrieved absolute TEC profiles are shown in Fig. 8. The black and red curves are derived by using Eqs. (1a) and (1b), respectively. Due to the low accuracy of pseudorange, the black curves have larger perturbations than red curves. The profiles in panels (a), (b), and (e) only have TEC with positive elevation angle and in panels (c), (d), and (f) have both negative and positive and the can be used to retrieve electron density profiles. Many signals from different GNSS satellites are recorded in the file for the POD observations at the same time. When the observation has both GPS
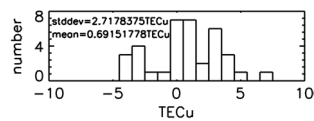

Fig. 8 Six examples of absolute TEC profiles of the F7/C2 TGRS retrieved from TROPS. The black and red curves show the TEC retrieved from pseudorange and phase, respectively. The information is recorded in **a** podTc2_F701.2020.099.00.55.R18_0001.0001_nc; **b** podTc2_F702.2020.099.01.36.R14_0001.0001_nc; **c** podTc2_F703.2020.099.06.24.G15_0001.0001_nc; **d** podTc2_F704.2020.099.10.52.G11_0001.0001_nc; **e** podTc2_F704.2020.099.19.13.R15_0001.0001_nc; **f** podTc2_F706.2020.099.15.00.G31_0001.0001_nc

Fig. 9 Number distribution of TEC difference between GPS and GLONASS satellites received by TGRS. The angle between GPS to F7/C2 and GLONASS to F7/C2 is less than 3° at the same time from day of year 001 to 100 in 2020. A total of 36 pairs of absolute TECs are found and the mean and standard deviations of the difference are around 0.7 TECu and 2.7 TECu, respectively

and GLONASS signals at the same time and the angle between the GPS to F7/C2 and GLONASS to F7/C2 is smaller than 3° it is retrieved as the absolute TEC product, and the GPS and GLONASS absolute TEC pair is used for comparison. From day of year 001 to day of year 100 in 2020, around 36 such pairs are found. The numerical distribution of the difference between GPS and GLONASS absolute TEC is shown in Fig. 9. The mean difference and the standard deviation of the TEC difference between the GPS and GLONASS signals are around 0.7 TEC units (TECu) and 2.7 TECu. The small TEC difference between GPS and GLONASS can validate the absolute TEC of the TROPS retrieval.

4 Conclusions

TROPS is a Taiwan built data processing system for RO observation. After the launch of the six LEO satellites on June 25th, 2019, named F7/C2, TROPS began to provide F7/C2 ionospheric retrieval products in March, 2020. The F7/C2 mission provided three products for the ionosphere. Except for the S4 index, which was calculated on board the satellite, the details of the retrieval process for the electron density profiles and absolute TEC are described in this study. The retrieval method used in TROPS is almost similar to the method of CDAAC in TACC. However, the number of electron density profile of TROPS is usually more than CDAAC in TACC for around several hundred after 2020. The reason perhaps due to the electron density profile need at least around continuous 10 min observations for retrieving and sometimes one profile is separated into two continuous dumps and TROPS connects the two dump separated profile well. Users can freely obtain the F7/C2 ionospheric products retrieved by TROPS from the TACC (https://tacc.cwb.gov.tw/v2/en/trops_download.html) and Space Weather Operational Office (https://swoo.cwb.gov.tw/) website.

Author contributions
All authors read and approved the final manuscript.

Declarations

Competing interests
The authors declare that they have no competing interest.

Author details
[1]National Space Organization, National Applied Research Laboratories, Hsinchu, Taiwan. [2]Department of Civil Engineering, National Kaohsiung University of Science and Technology, Kaohsiung, Taiwan. [3]Nuclear Science and Technology Development Center, National Tsing Hua University, Hsinchu, Taiwan. [4]Taiwan Analysis Center for COSMIC, Central Weather Bureau, Taipei, Taiwan. [5]GPS Science and Application Research Center, National Central University, Taoyuan, Taiwan. [6]Space Weather Operational Office, Central Weather Bureau, Taipei, Taiwan.

References
Chang FY, Liu JY, Chang LC, Lin CH, Chen CH (2014) Three-dimensional electron density along the WSA and MSNA latitudes probed by FORMOSAT-3/COSMIC. Earth Planets Space 67:156

Chen C-Y (2008) The observation of plasmaspheric electron content by FORMOSAT-3/COSMIC, Master thesis, National Central University

Chen S-P, Bilitza D, Liu J-Y, Caton R, Chang LC, Yeh W-H (2017) An empirical model of L-band scintillation S4 index constructed by using FORMOSAT-3/COSMIC data. Adv Space Res 60:1015–1028

Cherniak IV, Zakharenkova I, Karankowski A, Shagimuratov II (2012) Plasmaspheric electron content derived from GPS TEC and FORMOSAT-3/COSMIC measurement: solar minimum condition. Adv Space Res 50(4):427–440

Foelsche U, Kirchengast G (2002) A simple "geometric" mapping function for the hydrostatic delay at radio frequencies and assessment of its performance. Geophys Res Lett 29(10):1473

Fong C-J, Shiau W-T, Lin C-T, Kuo T-C, Chu C-H, Yang S-K, Yen NL, Chen SS, Kuo Y-H, Liou Y-A, Chi S (2008) Constellation deployment for FORMOSAT-3/COSMIC mission. IEEE Trans Geosci Remote Sens 46(11):3367

Hsu CT, Matsuo T, Wang W, Liu JY (2014) Effects of inferring unobserved thermospheric and ionospheric state variables by using an Ensemble Kalman Filter on global ionospheric specification and forecasting. J Geophys Res Space Phys 119:9256–9267

Lee IT, Matsuo T, Richmond AD, Liu JY, Wang W, Lin CH, Anderson JL, Chen MQ (2012) Assimilation of FORMOSAT-3/COSMIC electron density profiles into a coupled thermosphere/ionosphere model using ensemble Kalman filtering. J Geophys Res 117:A10318

Lin CH, Liu CH, Liu JY, Chen CH, Burns AG, Wang W (2010) Midlatitude summer nighttime anomaly of the ionospheric electron density observed by FORMOSAT-3/COSMIC. J Geophys Res 115:A03308

Lin CY, Matsuo T, Richmond AD, Liu JY, Lin CH, Tsai HF, Araujo-Pradere EA (2015) Ionospheric assimilation of radio occultation and ground-based GPS data using non-stationary background model error convariance. Atmos Meas Tech 8(1):171–182

Lin CY, Matsuo T, Liu JY, Lin CH, Huba JD, Tsai HF, Chen CY (2017) Data assimilation of ground-based GPS and radio occultation total electron content for global ionospheric specification. J Geophys Res Space Phys 122:10876–10886

Liu JY, Tsai HF, Jung TK (1996) Total electron content obtained by using global positioning system. Terr Atmos Ocean Sci 7(1):107–117

Liu JY, Lin CY, Lin CH, Tsai HF, Solomon SC, Sun YY, Lee IT, Schreiner WS, Kuo YH (2010) Artificial plasma cave in the low-latitude ionosphere results from the radio occultation inversion of the FORMOSAT-3/COSMIC. J Geophys Res 115:A07319

Liu JY, Chen SP, Yeh WH, Tsai HF, Rajesh PK (2016) The worst-case GPS scintillations on the ground estimated by using radio occultation observations of FORMOSAT-3/COSMIC during 2007–2014. Surv Geophys 37:791

Phinney RA, Anderson DL (1968) On the radio occultation method for studying planetary atmospheres. J Geophys Res 73(5):1819–1827

Schreiner WS, Sokolovskiy SV, Rochen C, Hunt DC (1999) Analysis and validation of GPS/MET radio occultation data in ionosphere. Radio Sci 34(4):949–966

Tsai LC, Liu CH, Hsaio TY (2009) Profiling of ionospheric electron density based on FormoSat-3/COSMIC data: results from the intense observation period experiment. Terr Atmos Ocean Sci 20(1):181–191

Tseng TP, Chen SY, Chen KL, Huang CY, Yeh WH (2018) Determination of near real-time GNSS satellite clocks for the FORMOSAT-7/COSMIC-2 satellite mission. GPS Solut 22:47

Wickert J, Reigber C, Beyerle G, Konig R, Marquardt C, Schmidt T, Grunwaldt L, Galas R, Meehan TK, Melbourne WG, Hocke K (2001) Atmosphere sounding by GPS radio occultation: first results from CHAMP. Geophys Res Lett 28(17):3263–3266

Yeh W-H, Huang C-Y, Hsiao T-Y, Chiu T-C, Lin C-H, Liou Y-A (2012) Amplitude morphology of GPS radio occultation data for sporadic-E layers. J Geophys Res 117:A11304

Yeh W-H, Liu J-Y, Huang C-Y, Chen S-P (2014) Explanation of the sporadic-E layer formation by comparing FORMOSAT-3/COSMIC data with meteor and wind shear information. J Geophys Res Atmos 119:4568–4579

Yue X, Schreiner WS, Hunt DC, Rocken C, Kuo Y-H (2011) Quantitative evaluation of the low Earth orbit satellite based slant total electron content determination. Space Weather 9:S09001

Publisher's Note

Springer Nature remains neutral with regard to jurisdictional claims in published maps and institutional affiliations.